Optimizing Electronic Structure and Quantum Transport at the Graphene-Si(111) Interface: An Ab Initio Density-Functional Study

Ceren Tayran, Zhen Zhu, Matteo Baldoni, Daniele Selli, Gotthard Seifert, and David Tománek

Optimizing electronic structure and quantum transport at the graphene-Si(111) interface: An *ab-initio* density-functional study

Ceren Tayran,[1,2] Zhen Zhu,[1] Matteo Baldoni,[3] Daniele Selli,[3] Gotthard Seifert,[3] and David Tománek[1,*]

[1]*Physics and Astronomy Department, Michigan State University, East Lansing, Michigan 48824, USA*
[2]*Department of Physics, Gazi University, Teknikokullar, 06500 Ankara, Turkey*
[3]*Physikalische Chemie, Technische Universität Dresden, D-01062 Dresden, Germany*
(Dated: March 7, 2013)

We use *ab initio* density functional calculations to determine the interaction of a graphene monolayer with the Si(111) surface. We found that graphene forms strong bonds to the bare substrate and accommodates the 12% lattice mismatch by forming a wavy structure consisting of free-standing conductive ridges that are connected by ribbon-shaped regions of graphene, which bond covalently to the substrate. We perform quantum transport calculations for different geometries to study changes in the transport properties of graphene introduced by the wavy structure and bonding to the Si substrate. Our results suggest that wavy graphene combines high mobility along the ridges with efficient carrier injection into Si in the contact regions.

It is now common knowledge that Moore's law, which has correctly represented the unprecedented progress of Si-based electronics for decades, can no longer be sustained as device dimensions approach the atomic scale [1]. One way to proceed next is to augment Si circuitry by taking advantage of the exceptional carrier mobility in graphitic nanostructres including graphene or nanotubes [2, 3]. Successful utilization of hybrid devices involving graphene and silicon necessitates microscopic understanding of the morphology, electronic structure and transport at the Si-graphene interface. There is reason for concern that graphitic carbon may not provide the desired benefit in this case, since the favorable π-bonding character has been shown to change in graphene interacting with related SiC [4–11] and SiO$_2$ [12–14] surfaces. So far, only a limited number of studies have investigated the interaction between graphene monolayers and pure Si. Except for a recent report of successful exfoliation of graphene on ultra-clean Si(111) [15], most studies focussed on Si(100) [16–19], where the symmetry difference between the overlayer and the substrate raises concerns about epitaxy and contact quality.

Here we study the electronic properties and quantum conductance at the graphene-Si(111) interface. We use *ab initio* density functional theory (DFT) to determine the equilibrium morphology of the interface and the nature of Si-graphene bonds. We find that the lattice mismatch between graphene and Si(111) can be accommodated by buckling the graphene overlayer and creating an array of free-standing graphene strips separated by regions covalently bonded to the substrate. Our ballistic transport calculations identify the effect of a covalently connected Si substrate on transport in the graphene overlayer and describe quantitatively the injection of carriers across the interface.

To gain insight into the equilibrium structure, stability and electronic properties of a graphene monolayer on
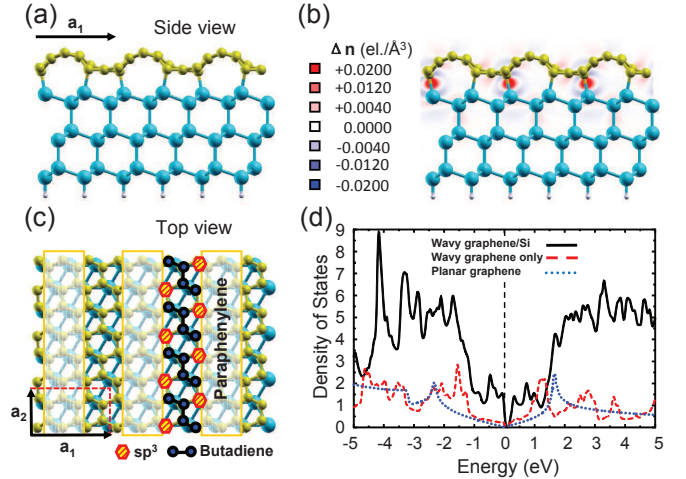

FIG. 1. (Color online) Optimum geometry and electronic structure of wavy graphene on the Si(111) surface. (a) Equilibrium structure of the slab and (b) electron density difference $\Delta n(\mathbf{r})$ in a plane normal to the surface. (c) Top view of the structure. The ridges of C atoms forming paraphenylene chains can be distinguished from sp^3 C atoms covalently bonded to Si and C atoms in butadiene like units that are not covalently bonded to Si. $\mathbf{a}_1$ and $\mathbf{a}_2$ are the Bravais lattice vectors defining the 2×1 surface unit cell. (d) Electronic density of states (DOS) of wavy graphene/Si(111) (solid black line), wavy graphene only (dashed red line) and planar graphene (dotted blue line). $E = 0$ denotes the position of the Fermi level.

the Si(111) surface, we performed DFT calculations as implemented in the SIESTA code [20]. The surface was represented by a periodic array of 6-layer Si(111) slabs, separated by an 8 Å thick vacuum region, which were connected to a graphene monolayer at the top and terminated by hydrogen at the bottom, as seen in Fig. 1(a). We used the Ceperley-Alder [21] exchange-correlation functional as parameterized by Perdew and Zunger [22],

norm-conserving Troullier-Martins pseudopotentials [23], and a double-ζ basis including polarization orbitals. The reciprocal space was sampled by a fine grid [24] of $6\times12\times1$ k-points in the Brillouin zone of the primitive surface unit cell and its equivalent for larger supercells. We used a mesh cutoff energy of 100 Ry to determine the self-consistent charge density, which provided us with a precision in total energy of $\lesssim2$ meV/atom.

Transport properties were investigated using the nonequilibrium Green's function (NEGF) approach as implemented in the TRAN-SIESTA code [25]. Ballistic transport calculations for optimized structures were performed using a single-ζ basis with polarization orbitals, a 200 Ry mesh cutoff energy, and a $4\times60\times1$ k-point grid [24].

Even though silicon and carbon are very similar in many ways, graphene is not epitaxial with any silicon surface. Previous theoretical studies of graphene on the Si(100) surface [18], which has a different symmetry, have assumed that the large lattice mismatch may be accommodated by stretching or compressing laterally the graphene overlayer. Since the in-plane compressibility of graphene is rather low, the energy cost to enforce epitaxy in this way by far exceeds the energy gained by graphene bonding to silicon, indicating that graphene should not bond to Si(100).

Also on the Si(111) surface, which has the same six-fold symmetry as the graphene overlayer, there is a large 11.6% lattice mismatch between the overlayer and the substrate. On this substrate, however, there is an alternative way to maintain epitaxy that does not involve in-layer compression and still benefits from interface bonding. When attached to Si(111), the graphene overlayer with the larger lattice constant may buckle and transform to a superlattice that we call wavy graphene. The graphene/Si(111) superlattice with the smallest 2×1 unit cell is shown in Figs. 1(a) and 1(c). We should emphasize that the non-planar, wavy structure of graphene in our study is stabilized by strong bonds between sp^3 hybridized atoms in the overlayer and the substrate, which is very different from thermodynamically induced rippling observed in graphene on metal substrates[26]. Whereas the bare Si(111) surface is known to undergo a 7×7 surface reconstruction[27], no such structural change occurs at the graphene-Si(111) interface, since the dangling bonds of surface silicon atoms have been saturated by forming strong σ bonds to the graphene overlayer, as seen in Fig. 1(b). The rectangular surface unit cell, delimited by the lattice vectors $\mathbf{a}_1$ and $\mathbf{a}_2$, contains 12 C atoms in the graphene layer, 12 Si atoms arranged in 6 slab layers, and 2 terminating H atoms.

The major benefit of the wavy structure is the coexistence of ribbon-shaped conducting graphene ridges that are detached from the substrate and separated by ribbons of carbon atoms bonded to the substrate, enabling carrier injection across the interface. The detached graphene

ridges contain embedded paraphenylene chains partly resembling poly-perinaphtalene, and are labeled in this way in Fig. 1(c). The separating regions contain sp^3 carbon atoms covalently connected to the Si substrate and short carbon chains resembling butadiene.

Clearly, changing the period of the wavy graphene structure offers a new structural degree of freedom to the graphene overlayer. We have investigated the relative stability of 2×1, 4×1 and 6×1 supercells of the graphene/Si interface by keeping the bottom four Si layers of the slab in the optimum Si bulk geometry [28]. Our numerical results allow for a quantitative analysis of all energy terms associated with the Si-graphene bonding. We find that especially the sp^3 carbon atoms bind strongly to Si atoms directly underneath, with the 2.0 Å long Si-C bonds comparable to the 1.9 Å long covalent bonds in SiC. The covalent bond character is also reflected in the electron accumulation in the bond region, as seen in the electron density difference $\Delta n(\mathbf{r}) = n_{\mathrm{tot}}(\mathbf{r}) - n_{\mathrm{graphene}}(\mathbf{r}) - n_{\mathrm{Si(111)}}(\mathbf{r})$ plotted in Fig. 1(b). If we were to attribute the entire graphene-Si interaction to these bonds, each of them would contribute 1.62 eV towards the binding energy. Obviously, maximizing the number of such C-Si bonds is beneficial for the stability of the interface.

To achieve epitaxy, there is an initial energy investment associated with the transformation of a free graphene monolayer to a wavy graphene structure matching the substrate. Even though buckling is less costly than in-plane compression, the net energy cost can not be neglected due the large flexural rigidity and low in-plane compressibility of graphene. We find that this energy investment decreases with increasing lattice constant $\mathbf{a}_1$ or the corresponding size n of the $n\times1$ supercell, favoring large supercells [28].

The relatively most stable structure of graphene bonded to silicon results from an energetic compromise between maximizing the number of Si-C bonds and minimizing the buckling energy. Due to the dominant role of the strong Si-C bonds, we find that the structure with the small 2×1 supercells represents the best energetic compromise.

Graphene will form stable bonds with the silicon substrate, if the adsorption process is exothermic, i.e. if $\Delta E = E_{\mathrm{tot,graphene/Si}} - (E_{\mathrm{tot,graphene}} + E_{\mathrm{tot,Si}}) < 0$. In this expression, $E_{\mathrm{tot,graphene/Si}}$ is the total energy of the relaxed wavy graphene structure on Si(111), $E_{\mathrm{tot,graphene}}$ that of the equilibrium planar graphene monolayer, and $E_{\mathrm{tot,Si}}$ is the total energy of the relaxed Si(111) surface. Defining the average adsorption energy per carbon atom as $E_{ad} = -\Delta E/N_{\mathrm{C}}$, where N_{C} is the number of carbon atoms per unit cell, we find $E_{ad} = -0.45$ eV in the optimum case, as the buckling energy dominates over the covalent bonds at the interface. We also found that partial hydrogenation of the graphene layer makes the formation of a stable graphene superlattice on Si(111) energet-

ically much more affordable, as it reduces the adsorption energy penalty down to $E_{ad} = -0.12$ eV in case of 4 H atoms per C_{12} unit cell. We expect that additional constraints, such as a low density of defects including substitutional impurities and vacancies at the interface, should turn $E_{ad} > 0$, yielding a stable bonding geometry between graphene and the Si(111) surface.

In the following, we will turn to the electronic structure and transport in the optimum 2×1 superlattice with $C_{12}Si_{12}H_2$ unit cells, shown in Fig. 1. The calculated 1.56 Å corrugation of the wavy graphene normal to the surface is sufficient to electronically decouple the carbon atoms in the paraphenylene chains, constituting the ridges, from the Si substrate, whereas the remaining carbon atoms in the troughs should be strongly perturbed by the vicinity of Si.

The electronic density of states (DOS) of graphene in different environments is shown in Fig. 1(d). In comparison to the free-standing graphene monolayer, which is a semi-metal with a smooth DOS near E_F, free-standing wavy graphene displays more peaks that reminisce of van Hove singularities in 1D systems and are caused by a reduction of $pp\pi$ interactions normal to the ridges. Apart from the only 0.03 eV wide band gap near E_F, the DOS of wavy graphene is enhanced with respect to its planar counterpart in the ≈2 eV wide energy range around E_F that is significant for transport. An even larger DOS enhancement near E_F is seen for wavy graphene bonded to the Si(111) surface. Interaction with the substrate increases the fundamental band gap width to 0.13 eV, in analogy to graphene in contact with other semiconductor surfaces including SiC [5] and diamond [29]. Results of our Mulliken population analysis indicate a small electron transfer from silicon to graphene. Such a charge redistribution, which is is expected based on the higher electronegativity of C as compared to Si, turns the interface to a pn junction. We find that the extra 0.2 electrons per carbon atom are distributed rather evenly across the wavy graphene layer. These results all indicate that the hybrid graphene/Si(111) system may display interesting quantum transport behavior.

In order to determine, how contact to a silicon substrate may affect conduction in a graphene monolayer, we performed quantum transport calculations of wavy graphene on Si(111) and present our results in Fig. 2. We distinguished transport normal to the ridges in transport geometry A, shown in Figs. 2(a) and 2(b), from transport along the ridges in transport geometry B, shown in Figs. 2(d) and 2(e). We constructed the semi-infinite leads of wavy graphene using one cell replicas in geometry A and two cell replicas in geometry B. The scattering region consists of three replicas of the 2×1 wavy graphene/Si(111) unit cell, augmented by one additional unit cell of wavy graphene on each side to properly describe the evanescence of scattering states into the lead region. All Si dangling bonds on the surfaces perpendic-
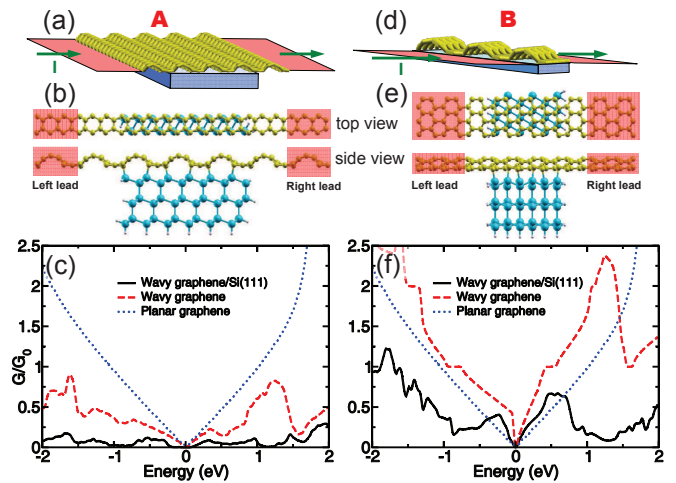

FIG. 2. (Color online) Setup for the quantum transport calculations for contiguous wavy graphene layers bonded to Si(111). Results for quantum transport normal to the ridges in transport geometry A (a-c) are compared to those along the ridges in transport geometry B (d-f). (a,d) Schematic geometry for the calculations, distinguishing perfect graphene leads from the central scattering region, with the direction of the current I shown by the arrows. (b,e) Atomic structure of the scattering region and its connection to the leads in top and side view. (c,f) Quantum conductance G in units of the conduction quantum G_0 as a function of injection energy, with $E = 0$ corresponding to the Fermi level. The conductance is given per unit cell normal to the transport direction, shown in panels (b) and (e).

ular to the transport direction have been saturated by H atoms. Both leads and the scattering region are infinitely wide and periodic normal to the transport direction.

Transmission spectra $G(E)$ of a contiguous graphene layer in different environments are shown in Fig. 2(c) for transport geometry A and in Fig. 2(f) for transport geometry B. In both cases, we compare the quantum conductance of wavy graphene in contact to Si(111) to that of free-standing wavy or planar graphene monolayers. Our results for geometry A indicate that transmittance normal to the graphene ridges in free-standing wavy graphene is reduced to some degree in comparison to planar graphene. The transmission spectrum of wavy graphene displays more peaks than that of planar graphene, reflecting the changes in the DOS in Fig. 1(d) including a narrow transport gap of $\lesssim 0.05$ eV. Si acts as a weak scatterer when connected to wavy graphene. This further reduces the conductivity of the wavy graphene layer and opens an ≈0.35 eV wide transport gap, somewhat larger than the 0.13 eV wide fundamental band gap of the system, seen in Fig. 1(d).

Electron transmission along the ridges of wavy graphene in transport geometry B, shown in Fig. 2(f), is greatly enhanced with respect to geometry A. Especially impressive is the conductivity enhancement in a free-standing wavy graphene monolayer over its free-
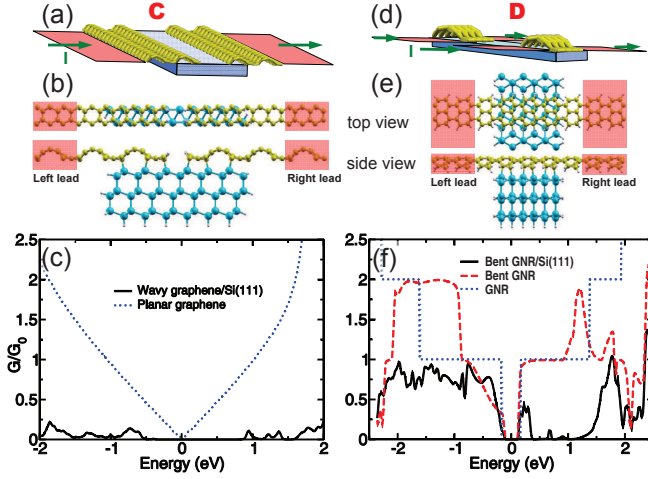
FIG. 3. (Color online) Geometry and quantum transport calculations for semi-infinite wavy graphene layers and graphene nanoribbons bonded to Si(111). Results in (a-c) are for transport geometry C analogous to that of Fig. 2(a), with the graphene monolayer disrupted by removing a ridge in the scattering region. Results in (d-f) are for transport geometry D analogous to that of Fig. 2(d), where removal of every other ridge resulted in the formation of bent graphene nanoribbons. (a,d) Schematic geometry for the calculations, distinguishing free-standing perfect graphene leads from the central scattering region, with the direction of the current I shown by the arrows. (b,e) Atomic structure of the scattering region and its connection to the leads in top and side view. (c,f) Quantum conductance G in units of the conduction quantum G_0 as a function of injection energy, with $E = 0$ corresponding to the Fermi level. The conductance is given per unit cell normal to the transport direction, shown in panels (b) and (e).

standing planar counterpart within a broad energy range, with the exception of a very narrow transport gap found also in geometry A. Even though attachment of the wavy graphene monolayer to Si reduces the net conductance of the system, this conductance is still higher than that of free-standing planar graphene in the ≈ 1 eV wide energy window near E_F that is most important for transport.

Results in Fig. 2 for transport geometry A and B confirm our hypothesis about the formation of anisotropic preferential transmission channels in wavy graphene, which are responsible for conduction enhancement along the conductive ridges containing embedded paraphenylene chains and suppression of conduction normal to these ridges.

To investigate the possibility of charge injection from graphene to silicon, we constructed transport geometry C by removing a ridge from wavy graphene in the scattering region of geometry A, as seen in Figs. 3(a) and 3(b). We followed the approach for geometry A in constructing the graphene leads and saturating all Si dangling bonds on the surfaces perpendicular to the transport direction by H atoms. In absence of the silicon substrate, there is obviously no transport due to the gap in a disrupted free-

standing wavy graphene monolayer. If there were no possibility to inject carriers across the silicon-graphene interface, this would also be true for the disrupted monolayer bonded to silicon. Our results in Fig. 3(c) suggest otherwise, as we do find transport channels passing through the silicon substrate. Obviously, carrier injection across the graphene-silicon interface is possible, albeit only into and from energetically allowed states below and above the 1.1 eV wide fundamental band gap of Si. As in the other transport geometries, the transport gap is larger than the fundamental band gap.

Finally, we followed up on our results for geometry B, which suggest enhanced conductance along ridges of wavy graphene, and studied the effect of laterally disconnecting the beneficial paraphenylene-based conductance channels. Transport geometry D, shown in Figs. 3(d) and 3(e), has been generated from geometry B by removing every other ridge of wavy graphene, creating an array of armchair graphene nanoribbons (GNRs) that are bent about their axis. These systems have been discussed widely as a viable alternative to zero-gap graphene [30, 31]. We constructed the graphene leads for GNRs and passivated the Si dangling bonds by hydrogen following the approach used for geometry B. Also the GNR edges were passivated by hydrogen.

Our transport results for an array of disconnected armchair GNRs in transport geometry D are presented in Fig. 3(f). The reference system, an array of planar 5-AGNRs, shows a constant conductance $G = 1G_0$ corresponding to one conductance channel in a $\gtrsim 2$ eV wide energy range around E_F, with the exception of an ≈ 0.3 eV wide transport gap. These findings agree with previously published electronic structure results [30, 31]. Transport properties of free-standing 5-AGNRs that are bent about their axis are very similar to the planar GNRs in a $1 - 2$ eV wide energy range around the narrow band gap. Attaching these GNRs to the Si(111) substrate causes a significant drop in conductance, especially in the conduction band region. This result is in stark contrast to the related transport geometry B that contains the same conductive paraphenylene-based ridges as geometry D, but does not separate them into nanoribbons.

The main message of our transport calculation is that especially in transport geometry B, the wavy graphene monolayer connected to a Si(111) surface may efficiently transport carriers along the graphene-silicon interface. Our results for geometry C indicate that the wavefunction overlap between the overlayer and the substrate is sufficiently large to permit carrier injection from graphene into the valence or conduction band of the silicon substrate.

In conclusion, we have studied the interaction of a graphene monolayer with the Si(111) surface using *ab initio* density functional calculations. We found that graphene forms strong bonds to the bare substrate and may accommodate the 12% lattice mismatch by forming

a wavy structure consisting of free-standing conductive ridges that are connected by ribbon-shaped regions of graphene, which bond covalently to the substrate. We performed quantum transport calculations for different geometries to study changes in the transport properties of graphene introduced by the wavy structure and bonding to the Si substrate. Our results suggest that wavy graphene combines high mobility along the ridges with efficient carrier injection into Si in the contact regions. This makes the hybrid graphene-silicon system a suitable candidate for a new generation of high-performance electronic circuitry.

* E-mail: tomanek@pa.msu.edu

[1] S. E. Thompson and S. Parthasarathy, Materials Today **9**, 20 (2006).

[2] P. Avouris, Z. Chen, and V. Perebeinos, Nature Nanotech. **2**, 605 (2007).

[3] K. Kim, J.-Y. Choi, T. Kim, S.-H. Cho, and H.-J. Chung, Nature **479**, 338 (2011).

[4] W. A. de Heer, C. Berger, X. Wu, P. N. First, E. H. Conrad, X. Li, T. Li, M. Sprinkle, J. Hass, M. L. Sadowski, M. Potemski, and G. Martinez, Sol. State Commun. **143**, 92 (2007).

[5] S. Y. Zhou, G.-H. Gweon, A. V. Fedorov, P. N. First, W. A. de Heer, D.-H. Lee, F. Guinea, A. H. Castro Neto, and A. Lanzara, Nat. Mater. **6**, 770 (2007).

[6] F. Varchon, R. Feng, J. Hass, X. Li, B. N. Nguyen, C. Naud, P. Mallet, J.-Y. Veuillen, C. Berger, E. H. Conrad, and L. Magaud, Phys. Rev. Lett. **99**, 126805 (2007).

[7] K. V. Emtsev, F. Speck, T. Seyller, L. Ley, and J. D. Riley, Phys. Rev. B **77**, 155303 (2008).

[8] S. Kim, J. Ihm, H. J. Choi, and Y.-W. Son, Phys. Rev. Lett. **100**, 176802 (2008).

[9] J. Hass, F. Varchon, J. E. Millán-Otoya, M. Sprinkle, N. Sharma, W. A. de Heer, C. Berger, P. N. First, L. Magaud, and E. H. Conrad, Phys. Rev. Lett. **100**, 125504 (2008).

[10] L. Magaud, F. Hiebel, F. Varchon, P. Mallet, and J.-Y. Veuillen, Phys. Rev. B **79**, 161405 (2009).

[11] C. Xia, S. Watcharinyanon, A. A. Zakharov, R. Yakimova, L. Hultman, L. I. Johansson, and C. Virojanadara, Phys. Rev. B **85**, 045418 (2012).

[12] M. Ishigami, J. H. Chen, W. G. Cullen, M. S. Fuhrer, and E. D. Williams, Nano Lett. **7**, 1643 (2007).

[13] E. Stolyarova, K. T. Rim, S. Ryu, J. Maultzsch, P. Kim, L. E. Brus, T. F. Heinz, M. S. Hybertsen, and G. W. Flynn, Proc. Natl Acad. Sci. **104**, 9209 (2007).

[14] P. Shemella and S. K. Nayak, App. Phys. Lett. **94**, 032101 (2009).

[15] O. Ochedowski, G. Begall, N. Scheuschner, M. E. Kharrazi, J. Maultzsch, and M. Schleberger, Nanotechnology **23**, 405708 (2012).

[16] K. A. Ritter and J. W. Lyding, Nanotechnology **19**, 015704 (2008).

[17] C.-C. Chen, M. Aykol, C.-C. Chang, A. F. J. Levi, and S. B. Cronin, Nano Lett. **11**, 1863 (2011), *ibid.* **11**, 5097 (2011)(E).

[18] Y. Xu, K. T. He, S. W. Schmucker, Z. Guo, J. C. Koepke, J. D. Wood, J. W. Lyding, and N. R. Aluru, Nano Lett. **11**, 2735 (2011).

[19] H. Yang, J. Heo, S. Park, H. J. Song, D. H. Seo, K.-E. Byun, P. Kim, I. Yoo, H.-J. Chung, and K. Kim, Science **336**, 1140 (2012).

[20] E. Artacho, E. Anglada, O. Dieguez, J. D. Gale, A. Garcia, J. Junquera, R. M. Martin, P. Ordejon, J. M. Pruneda, D. Sanchez-Portal, and J. M. Soler, J. Phys. Cond. Mat. **20**, 064208 (2008).

[21] D. M. Ceperley and B. J. Alder, Phys. Rev. Lett. **45**, 566 (1980).

[22] J. P. Perdew and A. Zunger, Phys. Rev. B **23**, 5048 (1981).

[23] N. Troullier and J. L. Martins, Phys. Rev. B **43**, 1993 (1991).

[24] H. J. Monkhorst and J. D. Pack, Phys. Rev. B **13**, 5188 (1976).

[25] M. Brandbyge, J.-L. Mozos, P. Ordejón, J. Taylor, and K. Stokbro, Phys. Rev. B **65**, 165401 (2002).

[26] A. L. Vázquez de Parga, F. Calleja, B. Borca, M. C. G. Passeggi, J. J. Hinarejos, F. Guinea, and R. Miranda, Phys. Rev. Lett. **100**, 056807 (2008).

[27] K. Takayanagi, Y. Tanishiro, M. Takahashi, and S. Takahashi, J. Vac. Sci. Technol. A **3**, 1502 (1985).

[28] See EPAPS Document No. ### for calculations addressing larger unit cells at different hydrogen coverages.

[29] Y. Ma, Y. Dai, M. Guo, and B. Huang, Phys. Rev. B **85**, 235448 (2012).

[30] K. Nakada, M. Fujita, G. Dresselhaus, and M. S. Dresselhaus, Phys. Rev. B **54**, 17954 (1996).

[31] Y.-W. Son, M. L. Cohen, and S. G. Louie, Phys. Rev. Lett. **97**, 216803 (2006), and *ibid.* **98**, 089901 (2007)(E).